TRACE ELEMENT PARTITIONING BETWEEN LOW-CALCIUM PYROXENE AND LUNAR PICRITIC GLASS MELTS AT MULTIPLE-SATURATION POINTS WITH APPLICATIONS TO MELTING AND MELT MIGRATION IN A HETEROGENEOUS LUNAR CUMULATE MANTLE. C. Sun and Y. Liang, Department of Geological Sciences, Brown University, Providence, RI 02912 (Chenguang_Sun@Brown.edu).

Introduction: Lunar mare basalts were formed by melting of the cumulate mantle [1]. They erupted on the lunar surface around 3.9 Ga to 3.2 Ga years ago (3.9-3.5 Ga for high-Ti basalts and 3.5-3.2 Ga for low-Ti basalts; [2]) and show a large range of major element composition (0.26-16.4% TiO_2; [1]). Low- and high-Ti mare basalts show distinct Hf-Nd isotope signatures, suggesting at least three chemical end-members exist in the lunar mantle (KREEP, high-Ti, and low-Ti cumulates; [3]). Geochemical studies indicate the presence of ilmenite in the high-Ti source region [1-7]. Addition of ilmenite in the lunar mantle may result from overturn of ilmenite-bearing late cumulate after lunar magma ocean (LMO) solidification [5]. However, ilmenite has not been observed at the multiple-saturation points of mare pristine glasses. Instead, olivine (ol) and low-Ca pyroxene are multiply saturated with picritic glass melts at pressure of 1.3-2.4 GPa and temperature of 1435-1560°C [8-12]. Consistent with crystallization of LMO [7], multiple-saturation experiments suggest that the mantle sources of mare basalts primarily consist of ol ± low-Ca pyroxene. Low-Ca pyroxene would have a greater contribution for trace element fractionation during melting of cumulate hybrid lunar mantle, and is important to understanding the petrogenesis of mare basalts.

The trace element partition coefficient (D) between mineral and melt is a function of pressure (P), temperature (T), and compositions of mineral and melt (X) [13]. As different mare basalts may have distinct cumulate mantle sources and melting paths, the P-T-X dependence of D in low-Ca pyroxene might lead to markedly different interpretations of magma genesis. To fully assess the fractionation of trace element in low-Ca pyroxene during magma genesis, we have developed a parameterized model for HFSE partitioning in low-Ca pyroxene in addition to our REE partitioning model [14]. By applying our partitioning models to low-Ca pyroxene at multiple-saturation points of the picritic glass melts, we show that D values of REE and HFSE in orthopyroxene (opx) or pigeonite vary by less than a factor of two for various melt and mineral compositions at multiple-saturation points. We employ a simple model to quantify mare basalt genesis, and show the importance of lunar source composition to petrogenesis of mare basalts.

A Predictive Model: Similar to REE, HFSE partition coefficients from a given mineral-melt partitioning experiment can be quantitatively described by the lattice strain model [13]. We have analyzed published Ti, Hf and Zr partitioning data between low-Ca pyroxene and basaltic melts under terrestrial and lunar conditions, and parameterized key partitioning parameters in the lattice strain model (D_0, r_0 and E) as functions of P, T and X. D_0 is found to positively correlate with Ca and Al abundance in low-Ca pyroxene, and negatively correlate with T. r_0 is positively correlated with Ca and Mg in low-Ca pyroxene. E is negatively correlated with r_0. Figure 1 shows the excellent agreement between the predicted and the observed REE and HFSE partition coefficients between low-Ca pyroxene and basaltic melt from partitioning experiments reported in the literature as well as those measured in our laboratory.

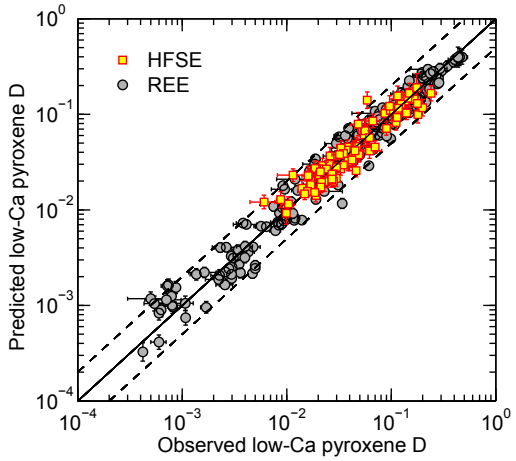

Figure 1. Predicted vs. observed D of REE and HFSE between low-Ca pyroxene and basaltic melt from partitioning experiments under terrestrial and lunar conditions. The predicted and observed D values tightly follow the 1:1 lines, suggesting excellent prediction of our REE and HFSE partitioning models for low-Ca pyroxene.

Multiple-saturation experiments have been used to determine the phase relations of a primary magma: its depth of origin, temperature, and mineralogy of the source region [8-12, 15]. These multiple-saturation points in P-T space may represent minimum or average depth in a polybaric melting process [15], and can be used to estimate mineral and melt compositions relevant to lunar magma genesis. Given the composition of low-Ca pyroxene, P and T, we can use our parameterized models to estimate REE and HFSE partitioning behavior in low-Ca pyroxene at multiple-saturation points. Figure 2 shows predicted D for REE and HFSE in low-Ca pyroxene close to multiple-saturation points

from phase equilibrium experiments for different lunar picritic glasses. The compiled *D* values from the literature vary by more than a factor of 10, which may significantly affect our interpretation of lunar mantle melting. Instead, the variations of estimated *D* values for opx or pigeonite are less than a factor of two at multiple-saturation points.

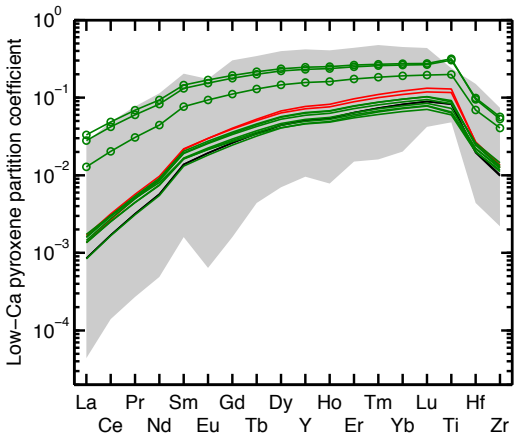

Figure 2. Predicted *D* for REE and HFSE in low-Ca pyroxene close to multiple-saturation points. Black, red, and green lines represent different starting compositions (black glass, red glass, and green glass, respectively) used in multiple saturation experiments. Lines with circle markers are pigeonite, and those without markers are opx. The gray region indicates the literature range of partitioning experiments.

A Simple Melting Model: To evaluate the effect of variations of *D* values in low-Ca pyroxene and source mineralogy on mare basalt petrogenesis, we use a simple 1-D model for trace element fractionation during melting and melt migration in a heterogeneous mantle [16]. We assume an ilmenite-bearing lherzolite for high-Ti source and a harzburgite for low-Ti source. The "enriched" component is KREEP in high- and low-Ti source regions. Hf and Nd isotope compositions of the sources are chosen from three end-members in Fig. 3a. Sm/Nd and Lu/Hf of the sources are calculated from Hf and Nd isotopes. Nd and Hf abundances of the three end-members are chosen from cumulate lunar mantle compositions [7]. In the model, melts are collected along the melting columns. We use the lowest and highest opx/melt *D* at multiple-saturation points in Fig. 2, and generate two sets of melts (dashed and solid lines in Fig. 3). Figure 3 compares calculated melts with mare basalts in terms of isotope and trace element compositions. In general, melts from different depth of melting columns can cover the observed trace element and isotope variations in mare basalts. Different opx/melt *D* at multiple-saturation points have little effect on isotope fractionation, but may change the trace element fractionation to less than 10%. Therefore, trace element *D* in low-Ca pyroxene may be taken as constant when modeling melting and melt migration in a hybrid lunar mantle. The three components in lunar mantle source may determine the first order variation in coupled trace element and isotope compositions of mare basalts.

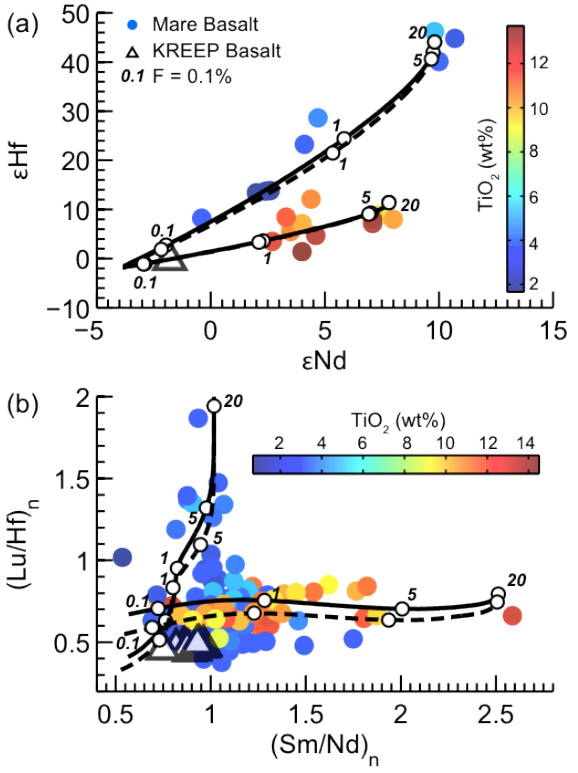

Figure 3. Variations of initial εHf and εNd of mare basalts and KREEP basalts (a) and variations of chondritic normalized $(Lu/Hf)_n$ and $(Sm/Nd)_n$ for mare basalts and KREEP basalts. Color dots represent mare basalts, and their color indices show TiO_2 contents. Triangles represent KREEP basalts. Black lines (dashed for lower *D* values and solid for higher D values) with circle markers show the melt compositions at different depths of the melting columns. Numbers close to circle markers represent the extent of melting (F).

References: [1] Delano (1986) *JGR*, 91, D201-D213. [2] Nyquist and Shih (1992) *GCA*, 56, 2213-2234. [3] Beard et al. (1998) *GCA*, 62, 525-544. [4] Liu et al. (2010) *GCA*, 74, 6249-6262. [5] Hess and Parmentier (1995) *EPSL*, 134, 501-514. [6] Papike et al. (1998) In: Planetary Materials. Chapter 5, pp1-234. [7] Snyder et al. (1992) *GCA*, 56, 3809-3823. [8] Green et al. (1975) *LPSC*, 6, 871-893. [9] Delano (1980) *LPSC*, 11, 251-288. [10] Wagner and Grove (1997) *GCA*, 61, 1315-1327. [11] Elkins et al. (2000) *GCA*, 64, 2339-2350. [12] Elkins-Tanton et al. (2003) *Meteoritics & Planet. Sci.*, 38, 515-527. [13] Blundy and Wood (1994) *Nature*, 372, 452-454. [14] Yao et al. (2012) *CMP*, in revision. [15] Longhi (1992) *LPSC*, 22, 343-352. [16] Liang and Parmentier (2010) *JP*, 51, 125-152.